Direct atomistic simulation of quartz crystal oscillators: Bulk properties and nanoscale devices

Jeremy Q. Broughton and Christopher A. Meli
Complex Systems Theory Branch, Naval Research Laboratory, Washington, D.C. 20375

Priya Vashishta and Rajiv K. Kalia
Physics Department, Louisiana State University, Baton Rouge, Louisiana 70803
(Received 29 May 1996; revised manuscript received 9 December 1996)

Current experimental research aims to reduce the size of quartz crystal oscillators into the submicrometer range. Devices then comprise multimillion atoms and operating frequencies will be in the gigahertz regime. Such characteristics make direct atomic scale simulation feasible using large scale parallel computing. Here, we describe molecular-dynamics simulations on bulk and nanoscale device systems focusing on elastic constants and flexural frequencies. Here we find (a) in order to achieve elastic constants within 1% of those of the bulk requires approximately one million atoms; precisely the experimental regime of interest; (b) differences from continuum mechanical frequency predictions are observable for 17 nm devices; (c) devices with 1% defects exhibit dramatic anharmonicity. A subsequent paper describes the direct atomistic simulation of operating characteristics of a micrometer scale device. A PAPS cosubmission gives algorithmic details. [S0163-1829(97)02126-7]

I. INTRODUCTION

Quartz crystal oscillators (QCO's) are used in a multitude of applications.[1,2] They are used as timing devices, as accelerometers, as mass balances, and as viscometers. Such devices can be excited in many different ways, but the one to be considered in this series of papers will be the ''flexural plate''; that is, one which oscillates by virtue of being plucked in the direction normal to the longitudinal axis. Conceptually they are the simplest of mechanical machines; they function like a violin string except that instead of catgut, they are made of quartz (SiO_2). The observed resonant frequencies are functions of the length of the device, its cross-sectional area, and its elastic constants (which, for an anisotropic material like α-quartz, vary with orientation). The latter, of course, are functions of temperature and degree of compression of the device.

Simple continuum elasticity theory[3] tells us that the frequencies (ω) should scale as

$$\omega \propto \frac{d}{L^2}\sqrt{\frac{Y}{\rho}}, \tag{1}$$

where Y is the Young's modulus of the material along the longitudinal direction. ρ is the density of the plate, L is its length, and d its thickness. Young's modulus gives the rate of change with elongation of longitudinal pressure in the rod when the two other directions are allowed to move freely in the hydrostatic bath. For our purposes, the hydrostatic pressure (**P**) will be one bar, which is very close to 1 atm. (Note that we boldface the symbol for pressure, because in general it will be a tensor). As regards the precision of molecular dynamics (MD), this pressure is essentially zero. The constant of proportionality in Eq. (1) depends upon the boundary conditions and eigenstate of the plate, for example, whether the ends are clamped or free to pivot.

It is easy to see that if internal loss mechanisms are kept to a minimum, such devices could operate as timing devices. If the device is put in an accelerating frame, with a reference mass at one end, it is also easy to see why they operate as accelerometers. Lastly, since density appears in Eq. (1), changing the mass of the device (via surface adsorption) also changes the frequency—hence they can function also as sensitive mass balances.

There is a technological drive to shrink the size of QCO's to the micrometer level. Present technology[4] makes them at the 100 μm scale, where they operate in the megahertz regime [substitution of appropriate values in Eq. (1) confirms this]. But the demand for further sensitivity is driving their size down. For example, oil companies would like gravitational detectors which are sensitive to nano-g's; present QCO's are sensitive to micro-g's. Such miniaturization is attendant with design issues: For example, increased sensitivity is achieved at the cost of increased noise. At what point does the statistical mechnical ''noise'' due to atomistics start to have an effect on device performance and reliability? For example, at what point does continuum elasticity theory [inherent in Eq. (1)] start to fail (and in what way) in determining device characteristics?

When a flexural plate shrinks to the micrometer scale (longitudinal axis) with typical aspect ratios of 10:1, the oscillation frequency is in the gigahertz regime. The number of atoms in such a system is in the tens of millions. Thus system sizes and time scales are appropriate for direct atomistic simulation on large scale parallel platforms such as those at DoD/DoE/NSF centers. Although existing interatomic potentials for SiO_2 are imperfect, they nevertheless contain enough of the physics and chemistry of the bonding that a direct simulation of a micron-sized device should reveal generic behavior which transcends the details of the potential and which would apply to a real device.

These, then, are the reasons for the present study. In this paper, we report results for the temperature-dependent be-

TABLE I. Elastic constants of α-SiO_2. Units of 10^5 bars.

	Bechmann (Ref. 22)	Mason (Ref. 23)	Present potential
c_{11}	8.674	8.605	6.945
c_{12}	0.699	0.505	1.927
c_{13}	1.191	1.045	2.121
c_{14}	-1.791	1.825	-0.175
c_{33}	10.720	10.710	7.459
c_{44}	5.794	5.865	3.222
c_{66}	3.988	4.050	2.401

havior of the bulk density and elastic constants. The latter are required to predict device frequencies from continuum elasticity theory. We continue by reporting results for the effective Young's modulus as a function of cross-sectional area of the SiO_2 plate (from which we develop a simple model to predict the asymptotic approach of the modulus to its bulk value) as well as frequencies obtained by direct simulation of a small device containing approximately 20 000 atoms, achievable on a dedicated workstation. We conclude by describing the effect of vacancies on device performance.

A subsequent paper will give results for direct simulation of a micrometer scale device performed on a parallel platform, namely the Air-force IBM SP2 at Maui. It will also present details of the domain decomposition for the parallel implementation.

In Sec. II, we describe the SiO_2 interatomic potential and the construction of the unit cell for both the bulk and device calculations. Section III gives a brief account of the multiple time step, constant pressure, constant temperature algorithm that we adopted for the bulk simulations. A full account of the algorithm is to be found in the accompanying PAPS submission.[5] Section IV presents results for the density, Young's modulus, and Poisson ratio as functions of the temperature for the bulk. Section V reports the Young's modulus versus the cross-sectional area of the SiO_2 flexural plate obtained via simulation. The section continues by fitting these to a simple model which allows asymptotic behavior versus cross-sectional area to be predicted. Section VI gives the frequencies obtained via direct simulation for a 17 nm plate and compares them with those predicted via continuum mechanics (CM). Finally, Sec. VII presents our conclusions.

II. SYSTEM AND INTERATOMIC POTENTIAL

The stable low-temperature, low-pressure phase of SiO_2 is that of alpha-quartz. It has a hexagonal unit cell comprising three silicons and six oxygens. Table I of the PAPS co-submission[5] gives the internal parameters of the basis according to Wycoff.[6] The particular orientation of the system in which we are interested is the so-called ''Z'' cut.[7] This way of cutting quartz ensures that the temperature dependence of the Young's modulus (or the linear expansivity) is zero near room temperature. Hence operating frequencies are insensitive to temperature with this cut. In Miller index parlance, this means that the faces of the plate will be: $(\bar{1},2,\bar{1},0)$, (0001), and $(1,0,\bar{1},0)$. Throughout the rest of this paper the y direction will represent the longitudinal direction of the plate; and the x direction will be that in which the plate has maximal amplitude (and in which the plate is thinnest). Thus the yx plane is the (0001), the yz plane is the $(\bar{1},2,\bar{1},0)$ and the xz is the $(1,0,\bar{1},0)$. Such an orientation allows, in the absence of fluctuations, a rectangular computational cell. For the purpose of the present bulk calculations, we simulated a system comprising 2592 atoms, with periodic boundary conditions, approximately cubic in shape with computational cell lengths near 30 Å. In order to achieve a rectilinear cell, we double the original nine atom unit cell and then use $6\times4\times6$ of the subsequent unit cells to produce the 2592 atoms. We expect finite-size effects of the thus-obtained densities and elastic constants to be small and certainly within the precision necessary for meaningful comparison with frequencies obtained via direct simulation.

For the construction of the plate, we use the same unit cell as for the bulk, but with basis atoms shifted such that the plate surfaces contain oxygens as their outermost atoms; such surfaces have the lowest energy for this potential. Vapor surrounds the flexural plate in the x and z directions, whereas periodic boundary conditions are employed in the y direction. (In reality, the x and z are also periodic, there being 40 Å of vapor surrounding the plate in these dimensions).

Turning now to the interatomic potential, a wide range of such have been employed in the literature to describe the structure and phonon frequencies of crystalline silica. Some are simple pair potentials,[8–11] others are shell models,[12] and still others are three body.[13,14] Our potential is of the latter kind. We chose to use the form due to Nakano, Kalia, and Vashishta[15] because it is able to describe many of the properties of molten, crystalline, and amorphous quartz. Our potential is identical in form to theirs except that values of a few constants are slightly different. These differences were tuned so that specifically crystalline properties would be obtained more accurately. The total potential energy is given as the sum of two-body and three-body terms:

$$V=\sum_{m<n} v_{mn}^{(2)}(r_{mn})+\sum_{l,(m<n)} v_{mln}^{(3)}(\mathbf{r}_{lm},\mathbf{r}_{ln}), \tag{2}$$

where r is the distance between atoms, and m and n designate atom indices. The two-body term is written as

$$v_{mn}^{(2)}(r)=A\left(\frac{\sigma_m+\sigma_n}{r}\right)^{\eta_{mn}}+\frac{Z_mZ_n}{r}e^{-r/\lambda} -\frac{\alpha_mZ_n^2+\alpha_nZ_m^2}{2r^4}e^{-r/\zeta}, \tag{3}$$

where the three terms represent short-range repulsion, Coulomb interaction due to ionicity, and a charge-induced dipole interaction caused by atomic polarizabilities, respectively. Note that the Coulomb and polarization terms are damped. Z is the nominal charge on the atom, α is the polarizability, and σ is a distance of ''closest approach.'' The two-body term is truncated at $r=r_c$ for ease of computation. For $r<r_c$, $v_{mn}^{(2)}$ is replaced by $v_{mn}^{(2)}(r)-v_{mn}^{(2)}(r_c)-(r-r_c)dv_{mn}^{(2)}/dr_c$, so that the value and its first derivative are zero at the cutoff. The three-body term is given by

$$v^{(3)}_{mln}(\mathbf{r}_{lm},\mathbf{r}_{ln}) = B_{mln}\exp\left(\frac{\xi}{r_{lm}-r_0}+\frac{\xi}{r_{ln}-r_0}\right)\left(\frac{\mathbf{r}_{lm}\cdot\mathbf{r}_{ln}}{r_{lm}r_{ln}} - \cos\overline{\theta}_{mln}\right)^2 \Theta(r_0-r_{lm})\Theta(r_0-r_{ln}), \quad (4)$$

where Θ is a Heaviside function. Notice that only the bond-bending terms of O-Si-O and Si-O-Si triplets are present in the Hamiltonian. Since diffusion is not important in this system, other triplets are unlikely to be important. The constants here are chosen to get the atomic positions and the bulk modulus right at $T=0$. Table II of the PAPS cosubmission reports all the potential constants,[5] but suffice it here to say that the only ones differing from Nakano *et al.*[15] are A (0.30608 eV), Z_{Si} (0.7872 e), Z_{O} (-0.3936 e), and $\overline{\theta}_{\mathrm{Si\text{-}O\text{-}Si}}$ (143.70 degrees). Their potential was optimized for amorphous silica; the changes here are required for the better description of crystalline quartz. The experimental (Wycoff) and relaxed $T=0$ basis vectors agree very well and are given in Table I of the PAPS cosubmission.[5] Table I compares two sets of experimental elastic constants with the fully relaxed $T=0$ values due to this potential. The overall bulk modulus of 3.736×10^5bar is fit exactly; whereas trends in the individual constants (c_{11} through c_{66}) are obtained qualitatively correctly. Note that the two experimental values for c_{14} are essentially equal but opposite in sign; this difference is still not resolved. For the purposes to which this potential will be put (namely, studying generic QCO behavior), we deem this potential satisfactory.

III. ALGORITHMIC DETAILS

Since we want to obtain the Young's modulus and density of our SiO_2 as a function of T at a constant pressure of 1 bar, it will be necessary to perform constant T, constant P simulations for the bulk. Also, since the range of the two-body and three-body terms are so very different (the three-body terms truncate after nearest neighbors), there will be a tremendous computational speed advantage in using multiple time step methods.

Briefly, we use a generalization of the (N,P,T) ensemble method due to Lill and Broughton[16] for the bulk calculations. Also, although we use only one Nose-Hoover thermostat[17,18] for the atomic degrees of freedom, we had to use a Nose-Hoover chain (due to Martyna, Klein, and Tuckerman[19]) of length 10 to achieve satisfactory thermostatting of the lattice degrees of freedom. Finally, we use the multiple time step method of Tuckerman, Berne, and Martyna.[20] In this there is an innermost loop where rapidly varying degrees of freedom are updated frequently and an outer loop where the more slowly varying are evolved in time. The evolution of the cell lengths and angles depend upon the difference $(\mathbf{P}-\mathbf{P}^{\mathrm{Req}})$; satisfactory pressure stability is only achieved when the cell degrees of freedom are placed in the outer loop. The simulational pressure is calculated via the virial. The accompanying PAPS submission gives comprehensive details of the algorithm.[5]

For the flexural plate calculations of Secs. V and VI, we use an (N,V,E) ensemble. As for the bulk, the multiple time step method of Tuckerman *et al.*[20] is used, involving this time only the atomic degrees of freedom. These equations of motion may be generated from those of the PAPS submission[5] by letting the mass of the thermostats and cell degrees of freedom go to infinity.

IV. BULK PROPERTIES

The quantities of interest are density, Young's modulus, and Poisson ratios. The latter are defined

$$Y = L_y\left(\frac{\partial P_{yy}}{\partial L_y}\right)_T, \quad (5)$$

$$u_x = -\sigma_x u_y,$$

$$u_z = -\sigma_z u_y, \quad (6)$$

where, as we have said, the direction of compression/elongation is along the y axis and the x and z directions are allowed to 'breathe'' in response to the 1 bar external hyrostatic pressure. The Poisson ratio measures the degree to which compression/elongation along one axis affects the length along another. Since SiO_2 is not isotropic the Poisson ratios, σ_x and σ_z, in the x and z directions will not be equal. u is the relative displacement ($\Delta L/L$, etc.). The derivatives inherent in Eqs. (5) and (6) are evaluated numerically. At each temperature, three simulations were performed corresponding to $P_{yy}=$ 1 and ±3000 bar. In each case, off-diagonal components of the pressure tensor were set to zero, while P_{xx} and P_{zz} were set to unity. A least-squares linear fit is then performed on these results to obtain Y, σ_x, and σ_z. Each simulation required a 3000 Δt equilibration followed by a 6000 Δt statistics phase. Results are not given above 580 K because a phase transition occurs to the β phase. Table III of the PAPS cosubmission demonstrates this to be the case.[5]

Figure 1 shows the dependence of density upon temperature. The error bars here are easily within the size of the symbols. Throughout the entire temperature range the angles between the cell vectors remain at 90°.

Figure 2 illustrates what happens to the computational cell lengths as a function of temperature and pressure. (For the sake of clarity of viewing, these distances are not represented as unit-cell lengths; to do so, the x, y, and z lengths of Fig. 2 should be divided by 6, 4, and 6, respectively). There are three curves for each direction corresponding to applied P_{yy} pressures of -3000, 1, and 3000 bars. The positive P_{yy} pressure gives rise to a smaller y length and larger x and z lengths. The slope of each line is positive, in contradistinction with what is observed in experiment. The reason why QCO's are oriented with the Z cut is that near room temperature, the thermal linear expansivity goes through an extremum which translates into a Young's modulus which is invariant to temperature.[7] In other words extremely good thermal stability is achievable under ambient conditions for these QCO's. We note that our system shows no such behavior. We have two explanations for this difference; the most obvious is that our interatomic potential, as we have already noted, is imperfect. But a more likely explanation is that these simulations are purely classical, whereas the phonon population at these temperatures is almost certainly determined by the Planck distribution. (A quick look at the high-

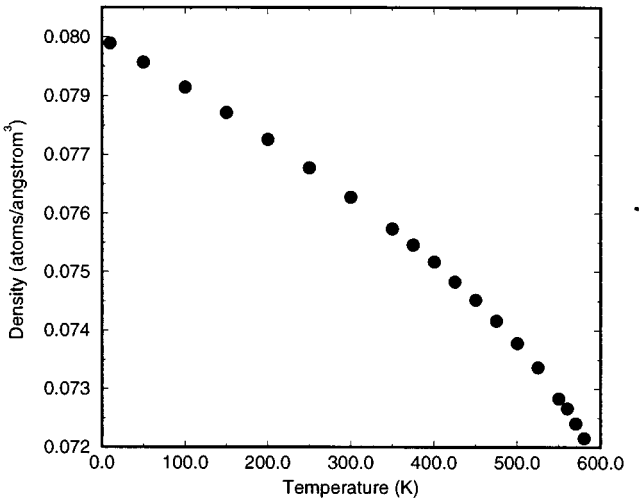

FIG. 1. Density versus temperature.

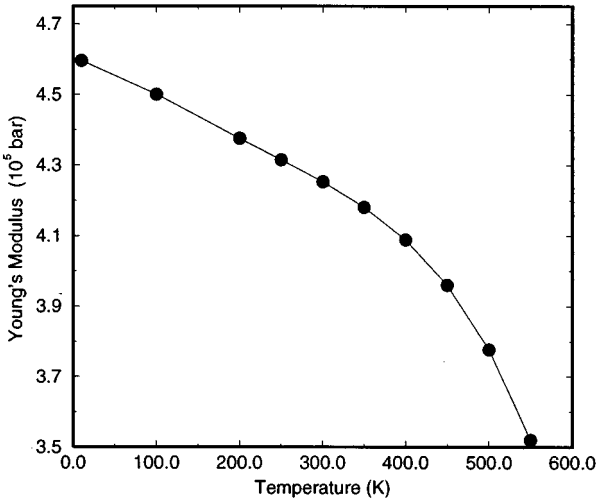

FIG. 3. Young's modulus versus temperature. Lines are to guide the eye.

frequency cutoff of any experimental quartz phonon spectrum indicates that the Debye temperature will be in excess of 1000 K (Ref. 21)). Although the statistical mechanics of long-wavelength acoustic modes is likely to be treated properly in these MD simulations, the high-frequency modes are almost certainly incorrectly treated and it may be their temperature-dependent population which leads to the experimentally observed invariance of the Young's modulus near 300 K.

The cell length information of Fig. 2, with the use of Eqs. (5) and (6), produces the Young's modulus and x and z Poisson ratios of Figs. 3 and 4. Notice that there is quite a strong variation of modulus with temperature, something that we require to know for accurate analysis of our direct device frequency evaluations.

V. PLATE MODULUS AND ANALYSIS

Systems in the submicrometer regime have large surface-to-volume ratios. A significant surface contribution to the effective Young's modulus of the device can be expected. It is the actual Young's modulus of the specific device which is required to predict, via continuum mechanics, the frequency of oscillation of the flexural plate. To quantify this, we evaluated the Young's modulus of flexural plates of varying cross-sectional area. We used a constant x:z aspect ratio of approximately 1:2 and evaluated the Young's modulus at $T=10$ and 300 K. Specifically, a constant number of seven y unit cells were employed and we varied the number of x and z cells subject to the constraint that the number of z cells was twice that of the x. The cells are defined in Sec. II above.

For each system size and temperature, the plate was equilibrated over 50 000 time steps for y cell lengths near $P_{yy}=0$. A further 50 000 steps were then employed to gather pressure statistics. A linear fit was then performed on the pressure versus length data to extract [see Eq. (5)] the Young's modulus. Note that in evaluating the pressure, the

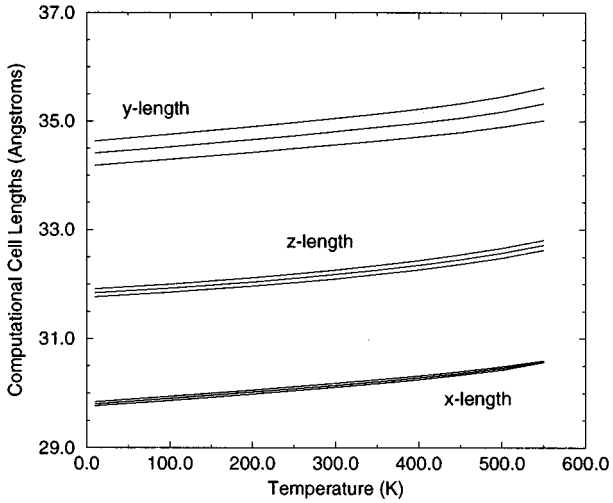

FIG. 2. Computational cell lengths versus temperature. See text.

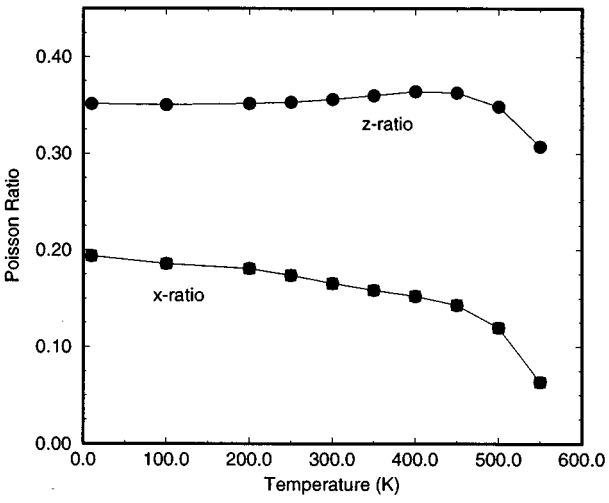

FIG. 4. Poisson ratios versus temperature. Error bars ± 0.02 at the highest temperature. Lines are to guide the eye.

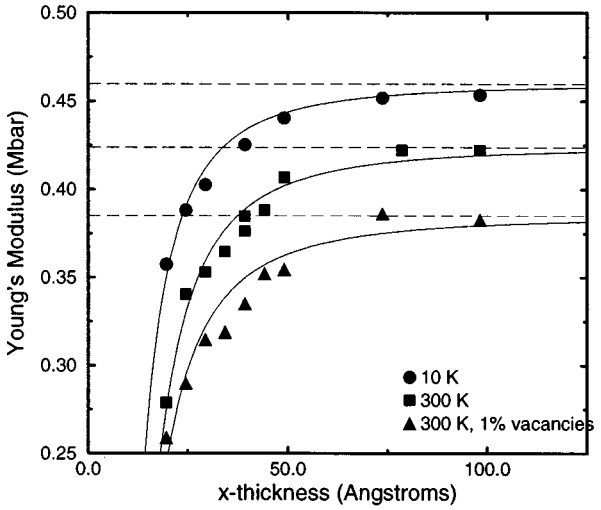

FIG. 5. Young's modulus versus x width for three different plates; 10, 300, and 300 K with 1% vacancies. x:z aspect ratio constant at 1:2. Continuous lines are from Eq. (8). Horizontal dashed lines are bulk limit.

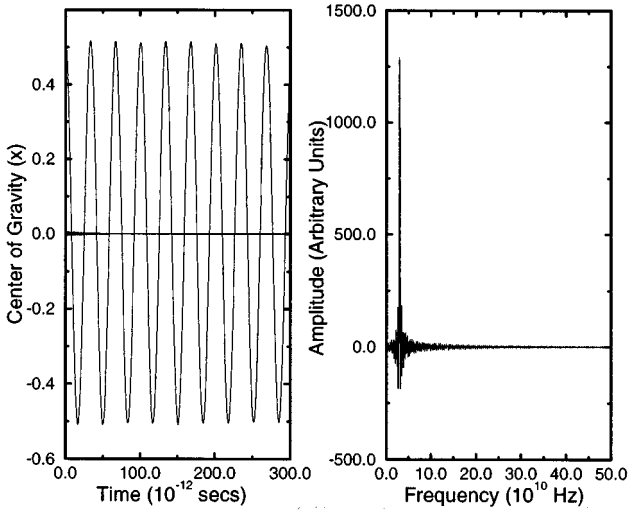

FIG. 6. Oscillation behavior of 10 K perfect plate. (a) Center of gravity versus time. Horizontal line is center of gravity of ends of plate. (b) Cosine transform.

volume used for the virial expression is that of the plate itself which is obtained from (a) the known length of the plate and (b) the cross-sectional area, A, defined by examining the density profiles in the x and z directions. Linear density profiles show oscillatory behavior in crystals; the outer maximum in each direction is used to define the width of the plate. For the purposes of the present analysis, any ambiguity in the definition of the volume of the plate is of little consequence in the analysis which follows. System sizes ranged up to 100 800 atoms ($20\times7\times40$ unit cells).

Figure 5 presents our raw data. Included also are results for a system with 1% of vacancies. Such vacancies are placed at random throughout the system and comprise both Si and O (in the ratio 1:2 to maintain charge neutrality). Such systems are of interest because commercial grade quartz, such as that used in many oscillator applications contain defects (hydrogen, aluminum, etc.) at similar levels (see Ref. 4). While we do not currently have useful Si, O, Al, H interacting interatomic potentials, we *can* ascertain the gross effects of defects at these concentrations by the simple expedient of using random vacancies.

In order to obtain the asymptotic behavior of modulus with increasing system size, it is necessary to fit this data to an appropriate analytic expression. In developing such, we imagine that the core of the plate has the bulk value (at given temperature) of the Young's modulus. We then assume that the surface skin has a different value for its modulus. We tried the following *ansatz* for the modulus of the bar:

$$Y = Y_B\left(\frac{A_B}{A_{\rm Tot}}\right) + Y_S\left(\frac{A_S}{A_{\rm Tot}}\right), \tag{7}$$

where subscripts B and S refer to bulk and surface, respectively. The cross-sectional area associated with the surface skin, assumes a surface skin depth. Of course, the sum of A_B and A_S must equal $A_{\rm Tot}$. This equation makes no distinction between the yx and yz surfaces; rather, it treats them as an average. For a given set of data (e.g., the 10 K data of Fig. 5), there is no unique best fit for Eq. (7) if both the skin depth and Y_S are allowed to vary as fitting parameters. Rather, one must be fixed. When this is done, the equation does not fit the data adequately.

The reason, we believe, is that corners (i.e., edges) of the plate are not properly treated. We therefore modified Eq. (7) thus

$$Y = Y_B\left(\frac{A_B}{A_{\rm Tot}}\right) + Y_S\left(\frac{A_S}{A_{\rm Tot}}\right) + Y_C\left(\frac{A_C}{A_{\rm Tot}}\right), \tag{8}$$

where subscript C refers to the corners. The sum of A_B, A_S, and A_C now equals $A_{\rm Tot}$. Again, for a given data set, there is no unique best fit if the skin depth, Y_S and Y_C are allowed to vary, but there is a best fit if the skin depth is fixed and the surface and corner moduli are allowed to vary. We set the skin depth to a value of 10 Å. This model now does fit the data satisfactorily, the result being shown as continuous lines in Fig. 5. The horizontal dashed lines represent the bulk asymptotes (from Sec. IV) to which the moduli must tend.

Table II gives the values of the fit to Eq. (8). Note that the arbitrary, but reasonable, choice of 10 Å for the skin depth produces surface Young's moduli slightly in excess of the bulk values. This should not be taken too literally; this is a fit to an *ansatz*, albeit one, we feel, which has physical basis. Larger values of the skin depth act to decrease Y_S.

The conclusion from this analysis is that for a plate with a typical aspect ratio of 1:14:2, the effective modulus of the bar will achieve 90% of the bulk value at 5.3×10^4, 95% at

TABLE II. Young's modulus fit for flexural plate according to Eq. (8). Moduli in units of Mbar.

	10 K plate	300 K plate	300 K plate, 1% vacancies
Y_B	0.460	0.424	0.385
Y_S	0.463	0.429	0.386
Y_C	0.223	0.101	0.082

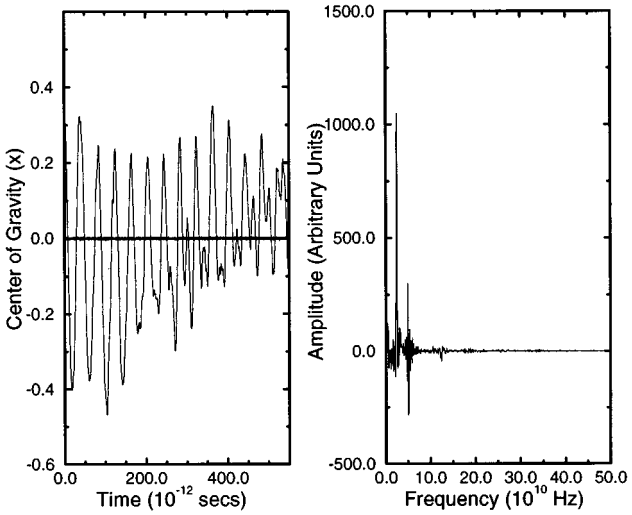

FIG. 7. Oscillation behavior of 300 K perfect plate. (a) Center of gravity versus time. Horizontal line is center of gravity of ends of plate. (b) Cosine transform.

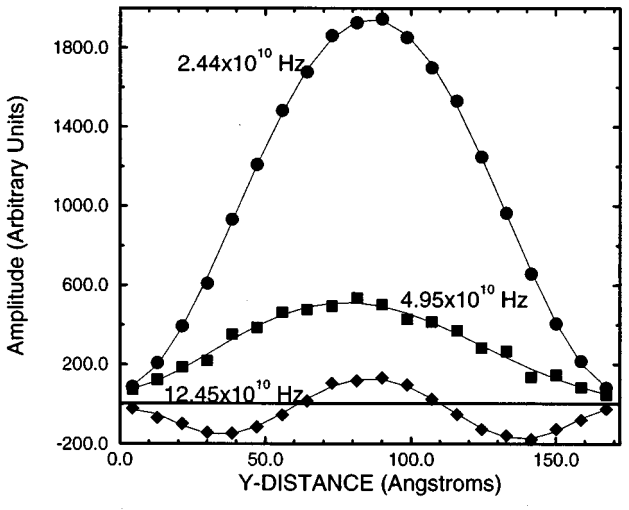

FIG. 8. Flexural modes of 300 K perfect plate. Data points fit with a sixth-order polynomial to guide the eye.

1.8×10^5, and 99% at 1.5×10^6 atoms. These conclusions are independent of temperature or of the vacancy concentration. These self-same atom numbers correspond to device lengths of 0.09, 0.13, and 0.26 μm, respectively. Thus the asymptotic approach to bulk elastic behavior is occurring in precisely the size regime to which next generation QCO's aspire. This general observation is unlikely to change with future improvements in the form of the SiO_2 interatomic potential.

Whether the actual oscillator frequencies converge on macroscopic behavior in the same size regime is the subject of a subsequent paper. Such calculations require the use of a parallel machine, but below we study an 18 000 atom (17.2 nm) plate whose simulation can be performed on a desktop workstation.

VI. DIRECT SIMULATIONS OF PLATES

The system comprised $5\times20\times10$ unit cells in the x, y, and z dimensions. The surfaces, as in the plate elastic constant calculations described above, were all oxygen terminated. We considered both perfect and 1% vacancy SiO_2 plates. Periodic boundary conditions are applied in all three directions, but with a vapor region surrounding the plate in the x and z dimensions. The center of gravity (CG) of the *y ends* of the plate are ''constrained'' in the x and z directions by adding two harmonic spring terms to the Hamiltonian of the system. Since the unperturbed plate's center of gravity is placed at (0,0,0) in our coordinate system, the two additional terms are $K\cdot(\mathrm{CG}_x)^2$ and $K\cdot(\mathrm{CG}_z)^2$ where K is a judiciously chosen spring constant. The center of gravity used in these expressions pertain to a y width of two unit cells at the ends of the plate (i.e., one at low values of y, the other at high). The effect of these soft constraints is to mimic the effect of clamps at either end of the plate. It would be possible to mimic further the effect of clamps by adding a random and disspiative heatbath to the ends, but this we chose not to do here.

After equilibration of each system at 10 and 300 K, such that the mean value of $\mathbf{P}_{yy}$ is near zero bar, their oscillatory motion was initiated by deforming (i.e., plucking) them in the x direction according to the continuum mechanical solution for a plate with clamped ends (which is distinct from a plate with freely pivoting ends). Such x displacement is of the form:

$$x(y)=Q[(\sin\kappa L_y-\sinh\kappa L_y)(\cos\kappa y-\cosh\kappa y)-(\cos\kappa L_y-\cosh\kappa L_y)(\sin\kappa y-\sinh\kappa y)] \quad (9)$$

and is applied to all atoms of the equilibrated undeflected state. Q is an amplitude factor. κ is obtained from the roots of

$$\cos\kappa L_y\cosh\kappa L_y=1, \quad (10)$$

the first three of which are 4.7300, 7.8532, and 10.9956. The characteristic frequencies are given (in radians/s) by

$$\omega=\frac{\kappa^2 d}{(\sqrt{12})L_y^2}\sqrt{\frac{Y}{\rho}}. \quad (11)$$

The appropriate Young's modulus to include here, of course, should be that which pertains to the plate, of given temperature and cross-sectional area, under consideration. Typical displacements at the midpoint of the plate are 1 Å, the plate being 172 Å long. This corresponds to less than 1° of deflection.

Figures 6 and 7 give the x center of gravity versus time and the associated cosine transform for the perfect plates at 10 and 300 K. (The center of gravity is for the entire plate). Notice firstly that the 10 K perfect system behaves very harmonically. The cosine transform gives a clean single peak at 3.05×10^{10} Hz. In contrast, the 300 K perfect plate's CG behavior is very clearly anharmonic and the Fourier transform indicates a principle peak at 2.44×10^{10} Hz with a

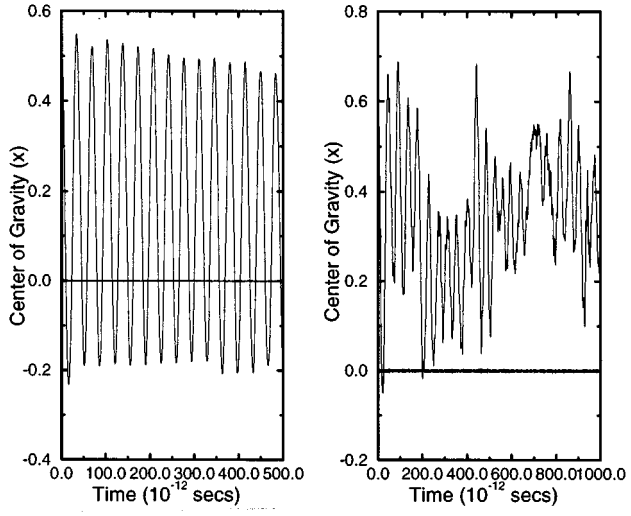

FIG. 9. Oscillation behavior of 1% vacancy plate. (a) Center of gravity versus time at 10 K. (b) Center of gravity versus time at 300 K. Horizontal lines are centers of gravity of ends of plate.

smaller but still significant one at 4.95×10^{10} Hz. There is also a feature at 12.45×10^{10} Hz. By dividing the plate into 20 y sections and monitoring the CG of each of these versus time, it is possible to determine to what modes these frequencies relate. Figure 8 shows the modes for the three freqencies. Note that the 2.44 and 4.95×10^{10} Hz states have a single maximum in the center of the plate, whereas the 12.45×10^{10} has two nodes.The 4.95×10^{10} state is therefore a second harmonic and the 12.451×0^{10} state represents the third excited state of the plate. No second excited state is present because it is disallowed by symmetry. Second harmonics are only allowed when significant anharmonicity is present.[3] The difference in behavior for the two temperatures is truly dramatic. We strongly suspect that, at the higher temperature, the motion of the surface atoms is highly anharmonic which, such is the large surface to volume ratio for these system sizes, couples significantly to the oscillatory dynamics of the whole plate.

Turning now to the systems with vacancies. Figure 9 shows, side by side, the dynamics of the 1% vacancy systems at both 10 and 300 K. The 10 K system appears very harmonic, but notice what has happened to the baseline. The amplitude fluctuations should be distributed equally around zero; that they are not shows that after the initial displacement, a memory of the event is stored in the system. In other words, significant plasticity occurs and the plate is permanently curved. In contrast, at 300 K, not only is the plate permanently curved, but also the oscillatory behavior is extremely anharmonic. The Fourier transforms (not shown) of these two systems produce a clean single-peak spectrum and a noisy multiple peak spectrum, respectively.

The frequency spectra obtainable via direct simulation can be compared with those predicted from continuum mechanics. The comparison is shown in Table III. The Young's modulus quoted is specific to the plate that was simulated. For this system size, the discrepancy between the continuum prediction and the frequency obtained via direct simulation would have been much larger if the *bulk* value of the modulus had been employed. As it is, we still see significant differences. At 10 K, there is a 10% difference, while at 300 K the difference is approximately 30%. The third state which is just determinable at 300 K (see Fig. 7) at 12.45×10^{10} Hz is to be compared with a prediction of 17.22×10^{10} Hz which constitutes a 38% difference.

TABLE III. Comparison of MD frequencies and those predicted by continuum mechanics. Moduli in Mbar. Frequencies in 10^{10} Hz.

System	Y	ω_{MD}	ω_{CM}
Perfect plate 10 K	0.388	3.05	3.36
Perfect plate 300 K	0.335	2.44	3.19
Vacancy plate 10 K	0.343	2.82	3.17

VII. CONCLUSIONS

This paper, together with the PAPS cosubmission,[5] has described an interatomic model suitable for the simulation of bulk crystalline quartz and for the description of quartz crystal oscillators. Even though this potential may not duplicate all the details of experimental quartz, there is sufficient physics contained therein that the qualitative details of how QCO's behave as a function of system size is likely to be correct. The paper has also described a multiple time step algorithm suitable for an (N,P,T) ensemble appropriate for bulk systems described by three-body potentials.

The principal objective here has been to obtain elastic properties germane to the analysis of the Z-cut oscillator frequencies directly evaluated in the latter part of the paper. These properties were obtained for bulk systems as well as for plate geometries as a function of plate cross-sectional area. We predict that asymptotic approach to within 1 elastic value occurs at device sizes just below 1 μm. Also, we find that for oscillators that are approximately 20 Å long, estimates of oscillator frequency based upon continuum mechanics, even when elastic constants appropriate for the specific device size under consideration are used, are in error by 10–30 % depending upon the temperature.

A by-product of this work has been to show that Poisson ratios in the directions normal to the ''Z cut'' are not isotropic and that the α to β transition is faithfully reproduced with our interatomic potential albeit at a temperature 270 K below experiment. (A brief description of the phase transition is given in the PAPS cosubmission.[5])

We have shown that evaluation of device frequency is possible via direct atomistic simulation and that whereas device behavior is very harmonic at $T=10$ K, the surface plays an important role in introducing anharmonicity at 300 K for 20 Å devices. Behavior of 0.1 μm devices is presently being studied by methods similar to those employed here on parallel machines. Such studies will be the subject of a future paper. We further showed that effects on device characteristics can be observed via atomistic simulation when defects at the 1% level are present.

ACKNOWLEDGMENTS

J.Q.B. wishes to thank ONR for partial support of this work and C.A.M. wishes to acknowledge the National Research Council for financial support.

[1] J.W. Grate, S.J. Martin, and R.M. White, Anal. Chem. **65**, 940A (1993).
[2] J.W. Grate, S.J. Martin, and R.M. White, Anal. Chem. **65**, 987A (1993).
[3] L.D. Landau and E.M. Lifshitz, *Theory of Elasticity* (Pergamon, Oxford, 1984).
[4] See, for example, *Proceedings of the IEEE International Frequency Control Symposium, San Francisco*, 1995 (IEEE, New York, 1995).
[5] See AIP Document No. E-PAPS/PRBMDO-56-611 for algorithmic details of the molecular-dynamics simulations. E-PAPS document files may be retrieved free of charge from our FTP server (http://www.aip.org/epaps/epaps.html) or from ftp.aip.org in the directory /epaps/. For further information: Electronic address: PAPS@aip.org or FAX: 516-576-2223.
[6] R.W.G. Wyckoff, *Crystal Structures* (Wiley, New York, 1963), Vol. 1.
[7] V.E. Bottom, *Introduction to Quartz Crystal Unit Design* (Van Nostrand Reinhold, New York, 1982).
[8] M.M. Elcombe, Proc. Phys. Soc. London **91**, 947 (1967).
[9] T.H.K. Barron, C.C. Huang, and A. Pasternak, J. Phys. C **9**, 3925 (1976).
[10] R.G.D. Valle and H.C. Andersen, J. Chem. Phys. **94**, 5056 (1991).
[11] S. Tsuneyuki, M. Tsukaada, H. Aoki, and Y. Matsui, Phys. Rev. Lett. **61**, 869 (1988).
[12] H. Schober, D. Strauch, K. Nutzel, and B. Dorner, J. Phys. Condens. Matter **5**, 6155 (1993).
[13] T. Pilati, F. Demartin, and C.M. Gramaccioli, Acta Crystallogr. Sec. B **50**, 544 (1994).
[14] M.E. Striefler and G.R. Barsch, Phys. Rev. B **12**, 4553 (1975).
[15] A. Nakano, R.K. Kalia, and P. Vashishta, J. Non-Cryst. Solids **171**, 157 (1994).
[16] J.V. Lill and J.Q. Broughton, Phys. Rev. B **49**, 11 619 (1994).
[17] S. Nose, Mol. Phys. **57**, 187 (1986).
[18] W.G. Hoover, Phys. Rev. B **34**, 2499 (1986).
[19] G.J. Martyna, M.L. Klein, and M. Tuckerman, J. Chem. Phys. **97**, 2635 (1992).
[20] M. Tuckerman, B.J. Berne, and G.J. Martyna, J. Chem. Phys. **97**, 1990 (1992).
[21] D. Strauch and B. Dorner, J. Phys. Condens. Matter **5**, 6149 (1993).
[22] R. Bechmann, Phys. Rev. **110**, 1060 (1958).
[23] W.P. Mason, *Piezoelectric Crystals and their Applications to Ultrasonics* (Van Nostrand, New York, 1950), p. 84.